Trilayered Block Copolymer Nanostructures Formed by an Iterative Layering Strategy

Pablo G Argudo, Nils Demazy, Guillaume Fleury

▶ **To cite this version:**

Pablo G Argudo, Nils Demazy, Guillaume Fleury. Trilayered Block Copolymer Nanostructures Formed by an Iterative Layering Strategy. Advanced Materials Interfaces, 2023, 10 (13), pp.2202493. 10.1002/admi.202202493 . hal-04094869

HAL Id: hal-04094869
https://hal.science/hal-04094869

Submitted on 11 May 2023

HAL is a multi-disciplinary open access archive for the deposit and dissemination of scientific research documents, whether they are published or not. The documents may come from teaching and research institutions in France or abroad, or from public or private research centers.

L'archive ouverte pluridisciplinaire **HAL**, est destinée au dépôt et à la diffusion de documents scientifiques de niveau recherche, publiés ou non, émanant des établissements d'enseignement et de recherche français ou étrangers, des laboratoires publics ou privés.

Trilayered block copolymer nanostructures formed by an iterative layering strategy

Pablo G. Argudo,[1,*] Nils Demazy, Guillaume Fleury[1,*]

[1]Univ. Bordeaux, CNRS, Bordeaux INP, LCPO, UMR 5629, F-33600, Pessac, France.

E-mail: pgomezargud@enscbp.fr, gfleury@enscbp.fr

Keywords: block copolymer, thin film layering, 3D hierarchical structures.

Abstract

Nanostructured block copolymer (BCP) thin films enable the formation on-demand of a variety of periodic patterns at the nanometer scale by tuning the macromolecular BCP characteristics and annealing processes. Significant progress in the control of the self-assembly has been witnessed over the past decade with the implementation of robust directed self-assembly methods. However, the self-assembled structural patterns obtained at equilibrium are limited and methods to expand the range of structural configurations are required to harness additional functionalities. Here, we demonstrate how PS-*b*-PMMA BCP thin layers can be stacked to produce a library of complex three-dimensional hierarchical heterostructures. In this iterative assembly process based on simple building bricks (i.e.; immobilized BCP patterns forming Holes, Lines and Dots), the stacking configuration (i.e. self-assembly and registration) of a BCP thin film is directed with respect to the previous layer using confinement effects and interfacial energy tuning. This responsive layering can lead to intricate three-dimensional Al_2O_3 structures and opens the way to a broad variety of structural designs toward functional applications.

1. Introduction

The self-assembly of block copolymers (BCPs) is the focus of intense research for the bottom-up fabrication of structures and patterns with nanometer-scale periodicity.[1–4] Indeed, the manufacturing of ordered nanostructures drives various fields of materials science with the implicit challenges of size reduction and geometrical variety of features. BCPs are formed by the covalent bonding of two or more macromolecular sequences,[5,6] and their self-assembly yields an array of phase-separated morphologies that can be selected through the BCP macromolecular characteristics (i.e. block chemical nature and sequence, molecular weight, composition, dispersity, etc.).[7,8] For instance, the simplest diblock architecture affords the generation of spherical, cylindrical, or lamellar structures which can be applied in thin film for the definition of well-ordered 2D arrays.[9–11] As a potential candidate for next-generation nanolithography,[3,12,13] nanostructured BCP thin films supplement conventional top-down fabrication methods for the development of masks,[14,15] sensors,[16,17] membranes,[18–20] nanoelectronics,[21–23] conductors,[24,25] or nanophotonics,[26] among others. Additionally, the soft matter-based periodic structures can be transferred into a substrate or converted into inorganic features (metal, metal oxide, etc.) through chemical transformation and/or selective removal of one of the BCP domains.[27–30] This bottom-up methodology has proven to be a versatile fabrication tool for the manufacturing of intricate cost-effective large-scale nanopatterns.[31,32] In this context, it is of great interest to achieve more complex geometrical patterns while having access to precise positioning of BCP features. Indeed, finely tailor-made structures can induce additional functionalities. For instance, complex dot arrays of metal nanoclusters patterned via BCP self-assembly were employed to decipher the electrocatalytic processes at an oxide electrode surface.[33] Another demonstration of interest is the manufacturing of moiré superstructures formed by stacked layers of dot arrays useful in the design of photonic metasurfaces with tunable optical properties.[34,35] However, the segregation behavior inherent to BCP self-assembly limits the achievable self-assembled geometrical patterns. Indeed, they are the

result of an energy-minimization process which tends towards the formation of structures minimizing the interface between BCP domains of different chemical nature.[5] An increase in the complexity of self-assembled geometrical patterns can be obtained via macromolecular engineering with the development of elaborated BCP architectures in the form of multiblock copolymers with different sequencing configurations (star, comb or cyclic copolymers).[36,37] Additional structuring fields such as dewetting,[38–40] mechanical or electromagnetic fields,[41,42] solvent vapor or thermal annealing,[43,44] or chemically or topographically patterned substrates[45,46] have also been shown to enlarge the span of geometrical features obtained by BCP self-assembly by stabilizing non-equilibrium configurations. Another strategy involves the stacking of nanostructured BCP films in order to create novel patterns.[47–49] Stacking of BCP layers were firstly used to induce increased orientational order for lamellar-forming PS-*b*-PMMA by capitalizing on the higher correlation length of cylinder-forming PS-*b*-PMMA.[50] This methodology leads to the development of three-dimensional (3D) nanostructures enabled by the immobilization of a first BCP layer via crosslinking.[51,52] Iterative self-assembly strategies were further refined through the development of advanced layering methods in order to generate non-native morphologies including mesh arrays or and complex 3D morphologies.[17,25,53–57] For instance, Russell *et al.* have recently demonstrated how “primed” self-assembly states obtained from stratified BCP bilayers can lead to non-native structural motifs by quenching intermediate ordered states during the self-assembly process.[58] These multilayered structures can further demonstrated increased functionality as shown by Cheng *et al.* with the fabrication of super-hydrophobic silica-like coatings obtained by the stacking of cylinder forming polystyrene-*b*-poly(dimethyl siloxane) BCPs with different periodicity.[57] Another example of functionality induced by the engineered stratified layers is the nano-manufacturing of 3D electroactive ZnO nanomesh arrays obtained by a combination of iterative self-assembly and micro-dose infiltration synthesis showing tunable electrical conductance with the number of stacked layers.[17]

Recently, we have demonstrated how the stacking configuration of PS-*b*-PMMA lamellar thin films can be controlled using confinement effects and interfacial energy fields.[59] We established a unique set of preferential registration relationships by adjusting both parameters, leading to on-demand configurations between superposed line & space arrays derived from out-of-plane lamellar BCP structures. This concept relies on directing the BCP self-assembly using both chemically and topographically fields generated by an immobilized BCP layer previously deposited. Here, we extrapolated this concept to other BCP morphologies with the aim of exploring the formation of trilayered structures. Using a sequential deposition of simple building bricks (i.e.; Holes, Lines and Dots) generated from BCP self-assembly, PS-*b*-PMMA thin layers were "responsively" stacked[55] to generate a library of complex hierarchical heterostructures.

2. Results and discussion

Thin film and responsive layering method. The general process flow for sample preparation is depicted schematically in **Figure 1**a. A detailed explanation of the protocol is given in the experimental section. In brief, a thin film of PS-*b*-PMMA is spin coated and thermally annealed onto a PS-*r*-PMMA grafted Si substrate that promotes an out-of-plane orientation of the different BCP morphologies (The PS volume fractions, f_{PS}^{v}, of the grafted PS-*r*-PMMA chains resulting in the formation of out-of-plane lamellae, out-of-plane PMMA cylinders, and out-of-plane PS cylinders on a flat Si substrate were 0.7, 0.78, and 0.58, respectively). Indeed, the interfacial energy between the substrate and the BCP domains can be modified by grafted PS-*r*-PMMA chains leading to a controlled orientation of the BCP structure with respect to the substrate plane.[60,61] The PMMA domains of the patterns are then selectively infiltrated with Al_2O_3 by Sequential Infiltration Synthesis (SIS).[62,63] The obtained layer exhibits a subtle surface topography (amplitude *ca*. 2-4 nm) coincident with the BCP morphology after immobilization (**Figure S1**a,b). Finally, the PS

domains are partially etched by O_2 plasma, leading to an increase of the surface topography (amplitude *ca*. 6 nm) between the inorganic features and the PS domains (**Figure S1**c).

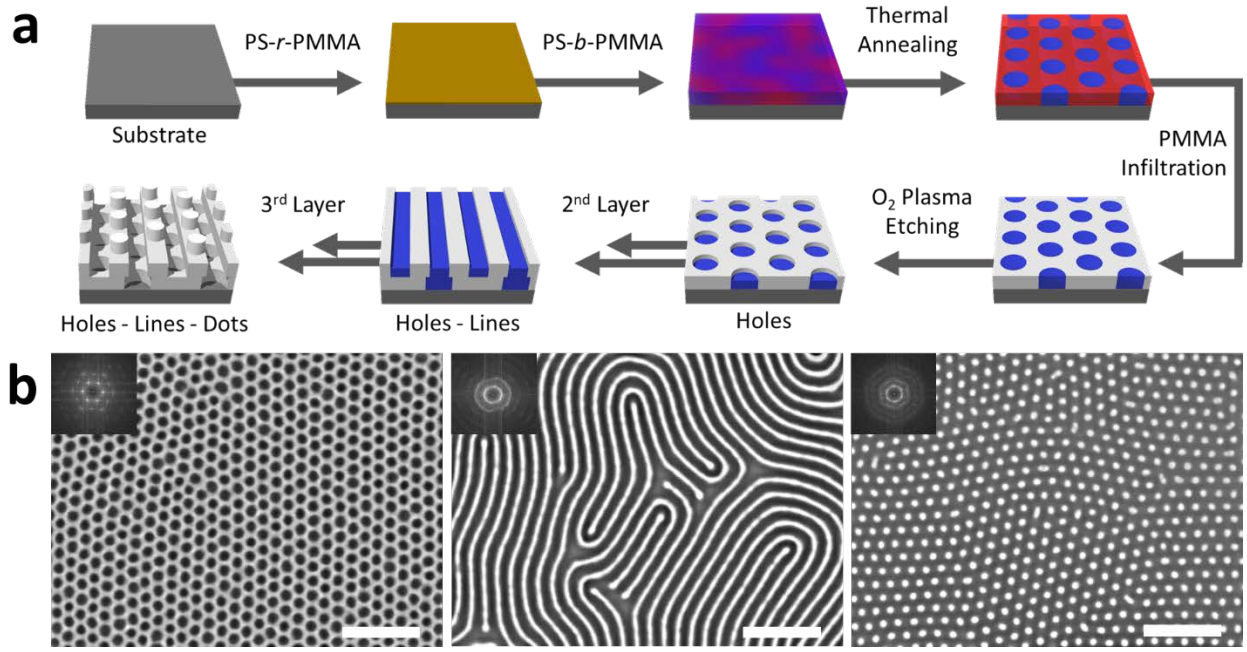

Figure 1. (a) Process flow for the formation of complex 3D structures via iterative self-assembly of BCP layers. (b) SEM top-view images of the building blocks after SIS with an intrinsic period of 32 nm. From left to right: Holes from out-of-plane PS cylinders, Lines from out-of-plane lamellae, Dots from out-of-plane PMMA cylinders. Scale bars are 200 nm.

This protocol was applied to three PS-*b*-PMMA BCPs of different compositions self-assembling in hexagonally packed PS cylinders (f_{PS}^{v}.= 0.27), lamellae (f_{PS}^{v}.= 0.51) and hexagonally packed PMMA cylinders (f_{PS}^{v}.= 0.69). Representative top-view SEM images of the final building blocks (i.e.; Holes, H; Lines, L; and Dots, D) with a common period, L_0, of 32 nm are given in **Figure 1**b (see **Figure S2**a for AFM characterizations of the various BCP monolayers after thermal annealing and **Figure S2**b for low magnification SEM images of the building blocks after SIS and O_2 plasma treatment). A similar protocol is followed for the stacking of the subsequent BCP layers, in which the underneath immobilized layer acts as a chemically and topographically patterned substrate for the following deposited one. In addition to the topographical field, the surface of the immobilized layer is modified by grafting PS-*r*-PMMA chains. Thereby the fine tuning of both parameters allow

a controlled registration between stacked BCP layers (i.e. a controlled positioning of the upper BCP domains with respect to the underlying pattern immobilized by SIS). Three interfacial configurations for the H, L and D building blocks were probed: a PMMA-Al_2O_3 affine registration, -m-; a "neutral" registration, -n-; and a PS-Al_2O_3 affine registration, -s- (see Table 2 for the composition of the PS-*r*-PMMA grafted layers used to induce the chemical field between the two layers). Significantly, regardless of the chosen interfacial configurations, the out-of-plane orientations of the BCP structures were preserved. Finally, the removal of the PS domains was performed using a prolonged O_2 plasma to ease the visualization by SEM of the 3D heterostructures.

3D morphologies. The responsive layering mechanism enables the formation of complex non-native patterns that expand the breadth of structures achievable using bottom-up BCP self-assembly. Indeed, the 3D configurations accessible by stacking multiple BCP layers are numerous *via* the variation of the structural motifs and their periodicity. In this study, we focused on building blocks with a periodicity, L_0, of 32 nm which were designed to assure commensurability between the different stacked patterns, and thus limit chain perturbations. As previously reported for bilayers of lamellar structures, we further demonstrate how the stacking configuration of PS-*b*-PMMA BCPs showing different morphologies can be directed with respect to a previous immobilized BCP layer using confinement effects and interfacial energy tuning. Here we were particularly interested by the formation of 3D trilayered structures for which three different chemical fields can be applied between the stacked layers. Indeed, the change of composition of the PS-*r*-PMMA grafted layer inserted between the BCP thin films yields the definition of three types of affinity for each probed BCP morphologies. It is thus possible to define a PMMA-Al_2O_3 (-m-), a PS-Al_2O_3 (-s-) or a neutral (-n-) affinity in order to study the registration mechanisms between the BCP layers. Notably, not all stacking configurations are accessible with the method described in this study. Indeed, some stacking configurations (i.e. L-s-L, D-s-D or L-s-D configurations) were found to be not

mechanically stable during the plasma treatment due to the collapse of the top structure inside voids created at the time of the plasma etching step (*vide infra*).

Firstly, we examined bilayered structures formed by the superposition of two patterns built with an interfacial chemical field described as PMMA-Al_2O_3 (-m-). Due to the responsive layering mechanism involving a PMMA-Al_2O_3 affinity, the PMMA domains of the 2nd layer positioned themselves in order to maximize the surface area with the underneath Al_2O_3 pattern. This behavior results in superimposed patterns for similar BCP structures (i.e., H-m-H, L-m-L or D-m-D) (see selected examples in **Figure 2**a,b, **Figure 4**a, and **Figure S3**a) or an "above" registration (i.e., maximizing the contacts between the Al_2O_3 pattern and the PMMA domains) for dissimilar BCP structures (i.e., H-m-L, H-m-D) (see selected examples in **Figure 3**a-c and **Figure S3**b). In contrast, when a PS-Al_2O_3 affine configuration is used, the PMMA domains of the 2nd BCP layer are positioned preferably over the pattern voids to favor contact between the Al_2O_3 and the PS domains (see selected examples in **Figure 2**c,d and **Figure S3**c). For instance, in this case of H-s-H bilayer, the PS domains of the top BCP layer registered along the vertices of the underneath hexagonal pattern in order to maximize contacts between the Al_2O_3 pattern and the PS domains. Finally, a neutral configuration between the layers leads to a registration mechanism directed by the topography of the underneath Al_2O_3 pattern. Accordingly, the examined L-n-L bilayered structure is constituted of two line & space patterns arranged in an orthogonal configuration. As previously demonstrated by Rahmann *et al.*, such configuration allows to relieve chain perturbations with respect to other stacking types leading to the formation of a grid pattern (see **Figure S3**d).[55]

These bilayered platforms were further used to examine the registration mechanisms of a third BCP layer as a function of the interfacial configuration. We particularly considered the H-m-H, H-s-H, H-m-L, L-m-L, L-n-L, and H-m-D bilayers as they provided mechanically robust platforms at the time of the ashing step used to reveal the trilayered structures. Indeed, bilayers and trilayers built based on a PS-Al_2O_3 interfacial field often result in the collapse of the hierarchical layered structures

due to the registration mechanisms favoring the positioning of the PMMA domains on top of the voids of the underneath Al_2O_3 pattern.

In **Figure 2**a-d, we used either H-m-H or H-s-H bilayers to stack an additional L or D pattern with a PMMA-Al_2O_3 interfacial field. For this particular configuration, the PMMA domains of the third layer maximize their coverage with the Al_2O_3 honeycomb pattern yielding immobilized Al_2O_3 lines or dots of the third layer positioned either along or above the vertices of the hexagonal pattern. Due to the commensurability between the different building blocks, the underneath pattern acts as a directing field for the lines or dots arrangement, preserving for instance the hexagonal symmetry of the dot pattern (see **Figure 2**b,d). Accordingly, two different configurations of lines-on-holes (H-m-H-m-L and H-m-H-s-L) and dots-on-holes (H-m-H-m-D and H-m-H-s-D) were fabricated depending on the interfacial fields.

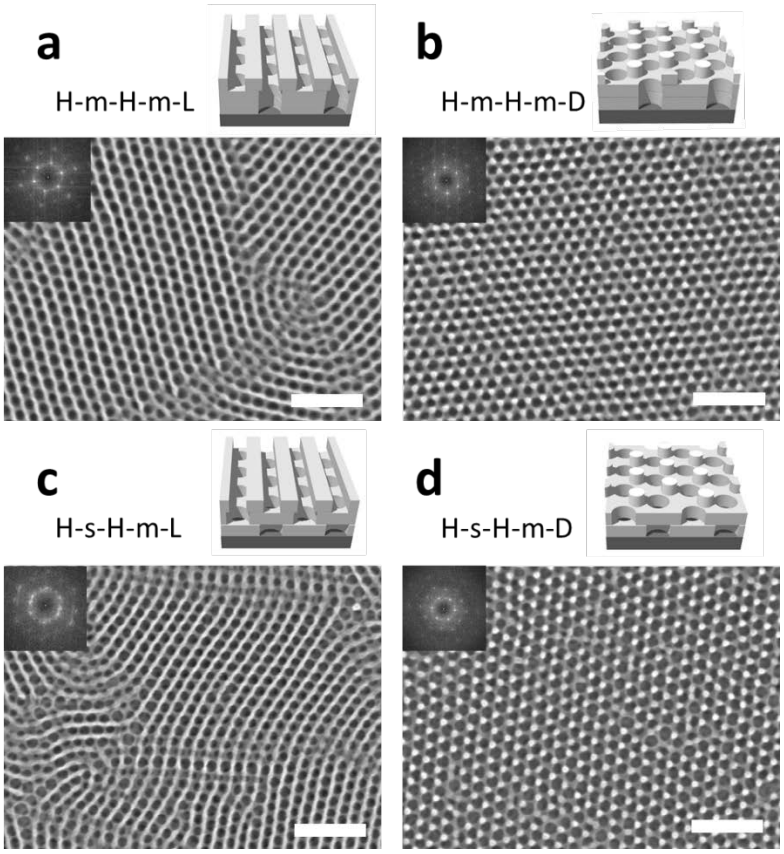

Figure 2. SEM top-view images of trilayered configurations based on Holes-on-Holes bilayers (Top left insets are the corresponding FFTs): (a) H-m-H-m-L, (b) H-m-H-m-D, (c) H-s-H-m-L, and (d) H-s-H-m-D. Scale bars: 200 nm.

We then explored trilayered structures based on immobilized H-m-L bilayers as shown in **Figure 3**a-c. By using a L pattern as a third layer with either a PMMA-Al_2O_3 or a neutral interfacial field, we respectively obtained a collinear or orthogonal configuration of the lamellar domains with respect to the underneath lines-on-holes structure as shown in **Figure 3**a,b. It is noteworthy that the H-m-L-n-L configuration generated a grid-on-hole pattern, highlighting the variety of structures achievable via iterative stacking. Finally, we used a dot pattern as third layer which was stacked on top of a H-m-L bilayered configuration using a PMMA-Al_2O_3 interfacial field (**Figure 3**c). The H-m-L-m-D configuration yield a lines-on-holes pattern decorated with dots which are positioned along the vertices of the hexagonal pattern *(vide infra)*.

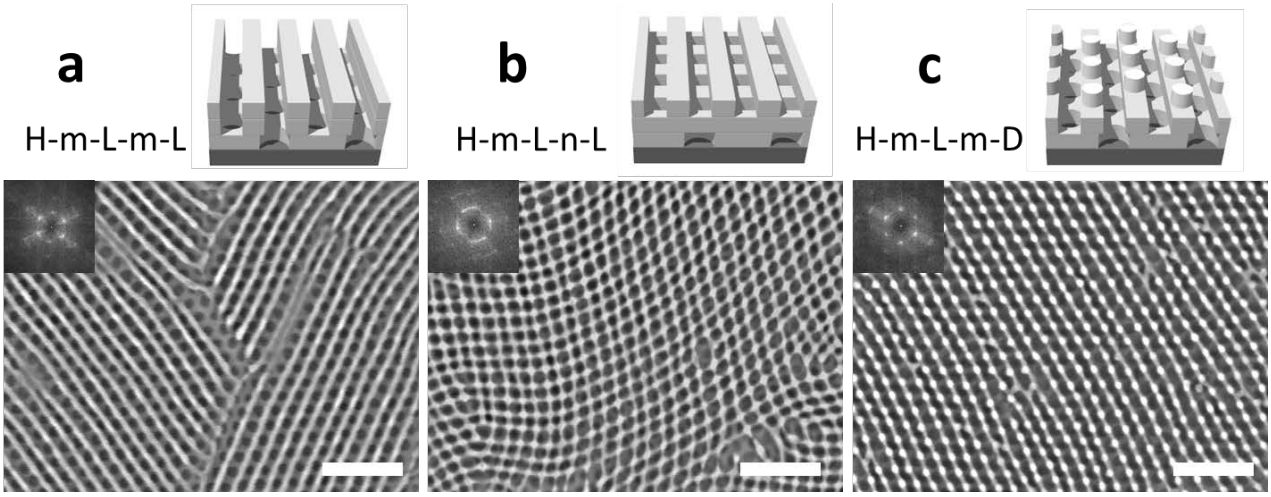

Figure 3. SEM top-view images of trilayered configurations based on Lines-on-Holes bilayers (Top left insets are the corresponding FFTs): (a) H-m-L-m-L, (b) H-m-L-n-L, and (c) H-m-L-m-D. Scale bars: 200 nm.

We further engineered trilayered based on L-m-L or L-n-L patterns as shown in **Figure 4**. The L-m-L-m-D stacking configuration results in a dots-on-lines structure while the L-n-L-m-D configuration produced an orthogonal grid pattern on which Al_2O_3 dots are positioned along the lines of the 2nd immobilized BCP layer. Interestingly, the position of the dots along the line or grid patterns for the H-m-L-m-D (**Figure 3**c) and L-n-L-m-D (**Figure 4**b), respectively, appears to be correlated with the first immobilized layer. Indeed, the dots of both structures are mainly positioned at either the vertices of the hexagonal pattern or the crossing points of the grid pattern. We supposed

that this behavior is related to a subtle topography induced by the stacking of the first two layers as the positioning of the dots on top of these bumps would relieve chain stretching.[55] Finally, we produced a trilayered mesh pattern using the L-n-L-n-L configuration as shown in **Figure 4**c. Due to the defective nature of BCP self-assembly, the expected mesh configuration depicted in the inset of **Figure 4**c is not fully retrieved and it is difficult to assess from the SEM images if an epitaxial registration is propagated through the stacked layers as in the case of H-m-L-m-D and L-n-L-m-D configurations. **Figure S4** shows the configuration of the L-n-L-n-L structure at each step of the stacking process (*i.e.* from the first immobilized layer to the final trilayered structure). While the formation of a grid with an orthogonal arrangement between the two first layers is readily visualized, the positioning of the third layer with respect to the first layer does not appear collinear.

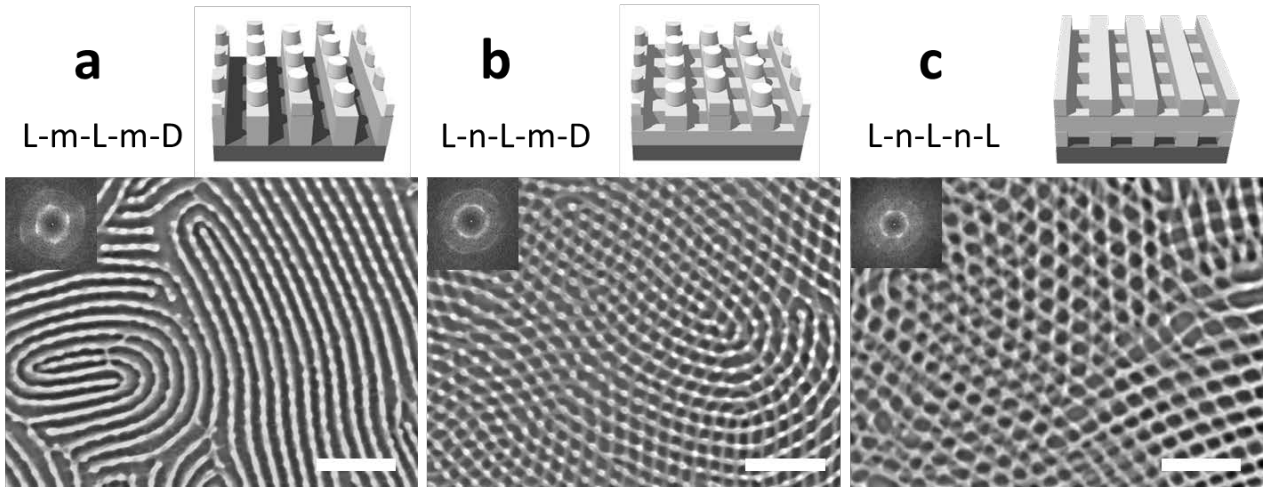

Figure 4. SEM top-view images of trilayered configurations based on Lines-on-Lines bilayers (Top left insets are the corresponding FFTs): (a) L-m-L-m-D, (b) L-n-L-m-D, and (c) L-n-L-n-L. Scale bars: 200 nm.

The aforementioned observations are a critical challenge for the iterative assembly strategy developed in this report. The polycrystalline nature of BCP self-assembly limits the correlation length of the self-assembled structures with the formation of grains with various angular orientations separated by grain boundaries.[64,65] The defectivity of a underneath immobilized BCP pattern further transfers to the subsequent stacked BCP structures. Accordingly, it appears important to

implement powerful directed self-assembly strategies (i.e. topographical or chemical templates obtained by photolithography enabling graphoepitaxy or chemiepitaxy) in order to induce long range ordering of the 1st immobilized BCP pattern. Indeed, the orientational and translational order of the subsequent BCP layers is strongly correlated with the one of the 1st immobilized layer. Interestingly, such interdependence can be used advantageously for particular stacking configurations such as H-m-L-m-L, H-m-L-n-L, and H-m-L-m-D. The faster coarsening kinetics of the hexagonally patterned underlying BCP layer can assist the lamellar alignment as demonstrated previously by Bang and coll.[52,66,67] This effect is clearly observed by comparing a neat Line pattern over a flat substrate (extracted correlation length of 142 nm) and a H-m-H-m-L stacking configuration (extracted correlation length 602 nm) as shown in **Figure S5**.

Finally, the proposed protocol leading to trilayered structures can be extended to the stacking of additional layers, demonstrating thus the robustness of this iterative strategy. As a proof of concept, the manufacturing of a tertralayered configuration consisting of H-s-H-m-L-m-D was attempted as shown in **Figure S6**. The retrieved configuration follows the same stacking rules as those observed for trilayered configurations with the dots of the fourth layer positioned on top of the lines of the third layer because of the PMMA-Al_2O_3 interfacial field used between the two layers.

3. Conclusions

In this work, we report the successful iterative stacking of various BCP patterns leading to complex 3D hierarchical structures. The tuning of the interfacial energy between the stacked BCP layers leads to the formation of multiple stacked configurations by using only three different BCP building patterns. The trilayered structures described in this study further demonstrated the robustness of the methodology based on the immobilization of BCP patterns by SIS in order to use it as a guiding template for the subsequent BCP layer using a combination of topographical and chemical fields. The commensurability between the line & space, honeycomb and dot patterns further enables

intricate responsive layering mechanisms for which the self-assembly of the top BCP layer ideally accommodated to the underneath immobilized Al_2O_3 pattern. This study holds promise for the generation of complex non-native structures in order to enrich the structural motifs accessible *via* BCP self-assembly in thin film. Furthermore, while this iterative stacking protocol is demonstrated for BCPs suitable for sequential infiltration synthesis, it could also be extended for BCP systems loaded *via* aqueous metal reduction (i.e. polystyrene-*b*-poly(2-vinyl pyridine) or polystyrene-*b*-poly(4-vinyl pyridine)) enabling the generation of oxide/metal patterns, useful for the future design of electronic and optical devices.[34,68]

4. Experimental Section

Polymer Materials. Polystyrene-*b*-poly(methyl methacrylate) (PS-*b*-PMMA) BCPs were obtained from Polymer Source and used as received. The macromolecular characteristics of the BCPs were confirmed by nuclear magnetic resonance spectroscopy and size-exclusion chromatography and the details are provided in **Table 1**. Throughout this work, BCP layers were denoted by the structural motif obtained after immobilization of the BCP structure (line & space pattern (L) from PS-*b*-PMMA forming lamellae; honeycomb pattern (H) from PS-*b*-PMMA forming PS cylinders; and dot pattern (D) from PS-*b*-PMMA forming PMMA cylinders).

Table 1. Macromolecular characteristics of PS-*b*-PMMA BCPs used in this study.

Pattern features	Holes (H)	Line (L)	Dots (D)
M_n [kg/mol]	56	45	48
f_{PS}^{v}	0.27	0.51	0.69
Đ	1.18	1.10	1.13

Morphology	Hexagonally packed PS cylinders	Lamellae	Hexagonally packed PMMA cylinders

Substrates. Silicon (100) substrates were used for the deposition of the BCP films, and their surface energy was tuned by grafting different PS-*r*-PMMA random copolymers (RCPs) or blends of RCPs provided by Arkema. The RCPs were synthesized by radical polymerization using BlocBuilder® MA-HEA-SG1 alkoxyamine. The PS volume fractions, f_{PS}^{v}, leading to the formation on a flat Si substrate of out-of-plane lamellae, out-of-plane PMMA cylinders, and out-of-plane PS cylinders were 0.7, 0.78, and 0.58, respectively. The grafting of RCP chains was performed by spin coating at 2 wt.% solution in propylene glycol methyl ether acetate (PGMEA) at 1500 rpm, followed by annealing at 230 °C for 5 min. The RCP-grafted substrates were subsequently washed in PGEMA before BCP deposition in order to remove ungrafted RCP chains.

Preparation of the nanostructured BCP films. BCP thin films were prepared by spin coating a 1.5 wt.% BCP solution in PGMEA onto the modified Si substrate or the immobilized BCP patterns at 2000 rpm. These coating conditions yield a film thickness of 25–35 nm (on flat Si substrate), which is in the monolayer or sub-monolayer regime. The BCP layers were thermally annealed using a rapid thermal annealing (RTA) tool (JetLight, Jipelec) under nitrogen in order to promote the self-assembly: 10 min at 230 °C out-of-plane lamellae, 15 min at 200 °C for out-of-plane PMMA cylinders, and 5 min at 260 °C for out-of-plane PS cylinders.

Sequential Infiltration Synthesis (SIS). The PMMA domains of the nanostructured BCP films were converted into Al_2O_3 by SIS using an atomic deposition layer (ALD) tool (Savannah G2, Veeco). Trimethyl aluminum (TMA) was used as the metallic gaseous precursor due to its strong selectivity to the PMMA domains.[69] Two cycles based on 2 TMA / 2 H_2O exposures (1 min exposure with a maximum pressure of around 15-20 mTorr for both precursors at 85 °C) and a purging step were used to infiltrate the PMMA domains and convert them into Al_2O_3.

Formation of multilayered structures. To obtain the 3D hierarchical structures, the underneath BCP layers infiltrated with Al_2O_3 were exposed to reactive ion etching (FLIRE300C, Plasmionique)) (40 W, 40 sccm O_2, 40 sec) in order to partially remove the PS domains, and thus create a surface topography. The resulting pattern was passivated by the deposition of a thin Al_2O_3 layer using 1 ALD cycle based on the sequential exposition of the surface to TMA and H_2O at 85 °C, leading to an Al_2O_3 layer thinner than 1 nm.[70] The passivated Al_2O_3 pattern was modified by grafting RCP chains with various PS volume fractions in order to define the pattern affinity with respect to the deposition of a subsequent BCP layer (see **Table 2** for the detailed compositions of the RCP layers used for the definition of the pattern affinity). Finally, a BCP thin film was deposited on top of the immobilized BCP layer, annealed, and infiltrated as described above. The process was then repeated for the formation of the trilayered structure as a function of the desired assembly of the third self-assembled BCP layer.

Table 2. Macromolecular characteristics of RCPs used for the definition of the surface affinity with respect to the BCP morphology.

Registration with respect to the BCP layer	RCP_A	RCP_B	A:B Blend Ratio
Neutral registration for out-of-plane lamellae (n-L)	f_{PS}^{v}= 0.69 Mn = 11.2 kg·mol^{-1}	f_{PS}^{v}= 0.75 Mn = 13.6 kg·mol^{-1}	3:1 f_{PS}^{v}= 0.7
PMMA-Al_2O_3 registration for out-of-plane lamellae (m-L)	f_{PS}^{v} = 0.63 Mn = 12.4 kg·mol^{-1}	f_{PS}^{v}= 0.49 Mn = 13.4 kg·mol^{-1}	3:1 f_{PS}^{v}= 0.6
PMMA-Al_2O_3 registration for out-of-plane PMMA cylinders (m-D)	f_{PS}^{v}= 0.69 Mn = 11.2 kg·mol^{-1}	—	—

PMMA-Al_2O_3 registration for out-of-plane PS cylinders (m-H)	f_{PS}^{v} = 0.40 Mn = 12.3 kg·mol^{-1}	—	—
PS-Al_2O_3 registration for out-of-plane PS cylinders (s-H)	f_{PS}^{v} = 0.63 Mn = 12.4 kg·mol^{-1}	—	—

Ashing. After the formation of the trilayered 3D nanostructure, the residual PS domains were removed by RIE using a prolonged O_2 plasma (40W, 20 sccm O_2, 9 min). Note that the eventual formation of Al_2O_3 in the RCP layer or through a generic ALD deposition mechanism does not prevent the removal of PS domains during the extended ashing step.

Imaging. Samples were characterized using scanning electron microscopy (SEM) and atomic force microscopy (AFM). SEM images were recorded using a JEOL 7800-E Prime at a 10 kV acceleration voltage. AFM images were obtained using a Dimension FastScan (Bruker) in tapping mode. Silicon cantilevers (Fastscan-A) with a tip radius of *ca.* 5 nm were used. The resonance frequency of the cantilevers was about 1400 kHz.

Supporting Information

Supporting Information is available from the Wiley Online Library or from the author.

Acknowledgments

N.D. is grateful for a financial support from the University of Bordeaux (Ph.D. fellowship). Arkema is acknowledged for supplying the PS-*stat*-PMMA materials. This work was supported by the REX-7 project (Région Rhône Alpes / BPI France), the French National Research Agency (Bonsai project ANR-21-CE09-0009), and the Equipex ELORPrintTec (ANR-10-EQPX-28-01).

References

[1] H.-C. Kim, S.-M. Park, W. D. Hinsberg, *Chem. Rev.* **2010**, *110*, 146.

[2] W. Li, M. Müller, *Prog. Polym. Sci.* **2016**, *54–55*, 47.

[3] C. M. Bates, F. S. Bates, *Macromolecules* **2017**, *50*, 3.

[4] C. Cummins, R. Lundy, J. J. Walsh, V. Ponsinet, G. Fleury, M. A. Morris, *Nano Today* **2020**, *35*, 100936.

[5] F. S. Bates, G. H. Fredrickson, *Annu. Rev. Phys. Chem.* **1990**, *41*, 525.

[6] N. Hadjichristidis, S. Pispas, G. Floudas, *Block Copolymers: Synthetic Strategies, Physical Properties, and Applications*, **2002**.

[7] V. Castelletto, I. W. Hamley, *Curr. Opin. Solid State Mater. Sci.* **2004**, *8*, 426.

[8] F. S. Bates, M. a Hillmyer, T. P. Lodge, C. M. Bates, K. T. Delaney, G. H. Fredrickson, *Science* **2012**, *336*, 434.

[9] L. Leibler, *Macromolecules* **1980**, *13*, 1602.

[10] M. W. Matsen, M. Schick, *Phys. Rev. Lett.* **1994**, *72*, 2660.

[11] M. W. Matsen, *Macromolecules* **2012**, *45*, 2161.

[12] S. Ji, L. Wan, C. C. Liu, P. F. Nealey, *Prog. Polym. Sci.* **2016**, *54–55*, 76.

[13] J. H. Kim, H. M. Jin, G. G. Yang, K. H. Han, T. Yun, J. Y. Shin, S. J. Jeong, S. O. Kim, *Adv. Funct. Mater.* **2020**, *30*, 1.

[14] C.-C. Liu, E. Han, M. S. Onses, C. J. Thode, S. Ji, P. Gopalan, P. F. Nealey, *Macromolecules* **2011**, *44*, 1876.

[15] C. M. Bates, M. J. Maher, D. W. Janes, C. J. Ellison, C. G. Willson, *Macromolecules* **2014**, *47*, 2.

[16] Y. S. Jung, W. Jung, H. L. Tuller, C. A. Ross, *Nano Lett.* **2008**, *8*, 3776.

[17] A. Subramanian, G. Doerk, K. Kisslinger, D. H. Yi, R. B. Grubbs, C. Y. Nam, *Nanoscale* **2019**, *11*, 9533.

[18] X. Feng, M. E. Tousley, M. G. Cowan, B. R. Wiesenauer, S. Nejati, Y. Choo, R. D. Noble, M. Elimelech, D. L. Gin, C. O. Osuji, *ACS Nano* **2014**, *8*, 11977.

[19] C. Zhou, T. Segal-Peretz, M. E. Oruc, H. S. Suh, G. Wu, P. F. Nealey, *Adv. Funct. Mater.*

2017, *27*, 1701756.

[20] S. Greil, A. Rahman, M. Liu, C. T. Black, *Chem. Mater.* **2017**, *29*, 9572.

[21] S. J. Jeong, S. Jo, J. Lee, K. Yang, H. Lee, C. S. Lee, H. Park, S. Park, *Nano Lett.* **2016**, *16*, 5378.

[22] C.-C. Liu, E. Franke, Y. Mignot, R. Xie, C. W. Yeung, J. Zhang, C. Chi, C. Zhang, R. Farrell, K. Lai, H. Tsai, N. Felix, D. Corliss, *Nat. Electron.* **2018**, *1*, 562.

[23] C. Cummins, M. A. Morris, *Microelectron. Eng.* **2018**, *195*, 74.

[24] J. Y. Kim, H. M. Jin, S. J. Jeong, T. Chang, B. H. Kim, S. K. Cha, J. S. Kim, D. O. Shin, J. Y. Choi, J. H. Kim, G. G. Yang, S. Jeon, Y. G. Lee, K. M. Kim, J. Shin, S. O. Kim, *Nanoscale* **2018**, *10*, 100.

[25] P. W. Majewski, A. Rahman, C. T. Black, K. G. Yager, *Nat. Commun.* **2015**, *6*, 7448.

[26] M. Stefik, S. Guldin, S. Vignolini, U. Wiesner, U. Steiner, *Chem. Soc. Rev.* **2015**, *44*, 5076.

[27] C. Liang, K. Hong, G. A. Guiochon, J. W. Mays, S. Dai, *Angew. Chemie - Int. Ed.* **2004**, *43*, 5785.

[28] N. L. Y. Wu, K. D. Harris, J. M. Buriak, *ACS Nano* **2013**, *7*, 5595.

[29] J. G. Werner, T. N. Hoheisel, U. Wiesner, *ACS Nano* **2014**, *8*, 731.

[30] C. Cummins, T. Ghoshal, J. D. Holmes, M. A. Morris, *Adv. Mater.* **2016**, *28*, 5586.

[31] R. A. Griffiths, A. Williams, C. Oakland, J. Roberts, A. Vijayaraghavan, T. Thomson, *J. Phys. D. Appl. Phys.* **2013**, *46*, 503001.

[32] G. Singh, S. Batra, R. Zhang, H. Yuan, K. G. Yager, M. Cakmak, B. Berry, A. Karim, *ACS Nano* **2013**, *7*, 5291.

[33] Y. Choi, S. K. Cha, H. Ha, S. Lee, H. K. Seo, J. Y. Lee, H. Y. Kim, S. O. Kim, W. C. Jung, *Nat. Nanotechnol.* **2019**, *14*, 245.

[34] K. Chen, B. B. Rajeeva, Z. Wu, M. Rukavina, T. D. Dao, S. Ishii, M. Aono, T. Nagao, Y. Zheng, *ACS Nano* **2015**, *9*, 6031.

[35] C. Jin, B. C. Olsen, E. J. Luber, J. M. Buriak, *ACS Nano* **2017**, *11*, 3237.

[36] V. P. Chuang, C. A. Ross, P. Bilalis, N. Hadjichristidis, *ACS Nano* **2008**, *2*, 2007.

[37] K. Aissou, W. Kwon, M. Mumtaz, S. Antoine, M. Maret, G. Portale, G. Fleury, G.

Hadziioannou, *ACS Nano* **2016**, *10*, 4055.

[38] S. M. Hur, M. S. Onses, A. Ramírez-Hernández, P. F. Nealey, J. A. Rogers, J. J. De Pablo, *Macromolecules* **2015**, *48*, 4717.

[39] F. Ferrarese Lupi, T. J. Giammaria, A. Miti, G. Zuccheri, S. Carignano, K. Sparnacci, G. Seguini, N. De Leo, L. Boarino, M. Perego, M. Laus, *ACS Nano* **2018**, *12*, 7076.

[40] H. Zhang, B. Wang, G. Wang, C. Shen, J. Chen, G. Reiter, B. Zhang, *Macromolecules* **2020**, *53*, 9631.

[41] C. Liedel, C. W. Pester, M. Ruppel, V. S. Urban, A. Böker, *Macromol. Chem. Phys.* **2012**, *213*, 259.

[42] P. W. Majewski, M. Gopinadhan, C. O. Osuji, *J. Polym. Sci. Part B Polym. Phys.* **2012**, *50*, 2.

[43] C. Sinturel, M. Vayer, M. Morris, M. A. Hillmyer, *Macromolecules* **2013**, *46*, 5399.

[44] D. Posselt, J. Zhang, D.-M. Smilgies, A. V. Berezkin, I. I. Potemkin, C. M. Papadakis, *Prog. Polym. Sci.* **2017**, *66*, 80.

[45] R. A. Segalman, H. Yokoyama, E. J. Kramer, *Adv. Mater.* **2001**, *13*, 1152.

[46] S. Ouk Kim, H. H. Solak, M. P. Stoykovich, N. J. Ferrier, J. J. de Pablo, P. F. Nealey, *Nature* **2003**, *424*, 411.

[47] C. A. Ross, K. K. Berggren, J. Y. Cheng, Y. S. Jung, J. B. Chang, *Adv. Mater.* **2014**, *26*, 4386.

[48] G. S. Doerk, K. G. Yager, *Mol. Syst. Des. Eng.* **2017**, *2*, 518.

[49] N. Demazy, C. Cummins, K. Aissou, G. Fleury, *Adv. Mater. Interfaces* **2020**, *7*, 1901747.

[50] R. Ruiz, R. L. R. L. Sandstrom, C. T. C. T. Black, *Adv. Mater.* **2007**, *19*, 587.

[51] E. Kim, C. Shin, H. Ahn, D. Y. Ryu, J. Bang, C. J. Hawker, T. P. Russell, *Soft Matter* **2008**, *4*, 475.

[52] H. Jung, D. Hwang, E. Kim, B.-J. J. Kim, W. B. Lee, J. E. Poelma, J. Kim, C. J. Hawker, J. Huh, D. Y. Ryu, J. Bang, *ACS Nano* **2011**, *5*, 6164.

[53] J. G. Son, A. F. Hannon, K. W. Gotrik, A. Alexander-Katz, C. a Ross, *Adv. Mater.* **2011**, *23*, 634.

[54] J. W. Jeong, Y. H. Hur, H. Kim, J. M. Kim, W. I. Park, M. J. Kim, B. J. Kim, Y. S. Jung,

ACS Nano **2013**, *7*, 6747.

[55] A. Rahman, P. W. Majewski, G. Doerk, C. T. Black, K. G. Yager, *Nat. Commun.* **2016**, *7*, 13988.

[56] C. Jin, B. C. Olsen, N. L. Y. Wu, E. J. Luber, J. M. Buriak, *Langmuir* **2016**, *32*, 5890.

[57] L. Cheng, J. W. Simonaitis, K. R. Gadelrab, M. Tahir, Y. Ding, A. Alexander-Katz, C. A. Ross, *Small* **2020**, *16*, 1905509.

[58] S. T. Russell, S. Bae, A. Subramanian, N. Tiwale, G. Doerk, C.-Y. Nam, M. Fukuto, K. G. Yager, *Nat. Commun. 2022 131* **2022**, *13*, 1.

[59] N. Demazy, P. G. Argudo, G. Fleury, *Small* **2022**, 2205254.

[60] P. Mansky, Y. Lui, E. Huang, T. P. Russell, C. J. Hawker, *Science* **1997**, *275*, 1458.

[61] E. Huang, S. Pruzinsky, T. P. Russell, J. Mays, C. J. Hawker, *Macromolecules* **1999**, *32*, 5299.

[62] M. Biswas, J. A. Libera, S. B. Darling, J. W. Elam, *Chem. Mater.* **2014**, *26*, 6135.

[63] Q. Peng, Y. C. Tseng, S. B. Darling, J. W. Elam, *ACS Nano* **2011**, *5*, 4600.

[64] H. Takahashi, N. Laachi, K. T. Delaney, S. M. Hur, C. J. Weinheimer, D. Shykind, G. H. Fredrickson, *Macromolecules* **2012**, *45*, 6253.

[65] W. Li, M. Müller, *Macromolecules* **2016**, *49*, 6126.

[66] H. Jung, S. Woo, S. Park, S. Lee, M. Kang, Y. Choe, J. G. Son, D. Y. Ryu, J. Huh, J. Bang, *Soft Matter* **2015**, *11*, 4242.

[67] S. Woo, H. S. Wang, Y. Choe, J. Huh, J. Bang, *ACS Macro Lett.* **2016**, *5*, 287.

[68] N. Yu, F. Capasso, *Nat. Mater.* **2014**, *13*, 139.

[69] Q. Peng, Y.-C. Tseng, S. B. Darling, J. W. Elam, *Adv. Mater.* **2010**, *22*, 5129.

[70] D. Pan, L. Ma, Y. Xie, T. C. Jen, C. Yuan, *J. Vac. Sci. Technol. A Vacuum, Surfaces, Film.* **2015**, *33*, 021511.

Table of Contents

An iterative self-assembly strategy using nanostructured block copolymer layers is used to generate complex trilayered nanostructures from three different structural motifs (honeycomb, line & space and dot patterns). Interfacial energy manipulations enable a fine control of the final structure by dictating the registration rules between the stacked BCP layers.